Spin-orbit-coupled Bose-Einstein condensates confined in concentrically coupled annular traps

Xiao-Fei Zhang,[1,2] Rui-Fang Dong,[1] Tao Liu,[1] W. M. Liu,[2] and Shou-Gang Zhang[1,*]

[1]*Key Laboratory of Time and Frequency Primary Standards, Chinese Academy of Sciences, Xi'an 710600, China*

[2]*Beijing National Laboratory for Condensed Matter Physics, Institute of Physics, Chinese Academy of Sciences, Beijing 100190, China*

(Received 8 October 2012; published 26 December 2012)

We investigate the ground state of spin-orbit-coupled Bose-Einstein condensates confined in concentrically coupled annular traps within the full parameter space accounts for all the nonlinear two-body collisions and the spin-orbit coupling. We find that depending on the ratio between interaction parameters and the strength of spin-orbit coupling, this coupled system presents various ground-state phases. Moreover, phase transition between radial phase separation and azimuthal phase separation can be induced by varying the strength of spin-orbit coupling when the system is first in radial phase separation, while phase transition between phase coexistence and azimuthal phase separation can also be realized through spin-orbit coupling when the system is first in phase coexistence. Finally, the spin texture is studied and the results show that the meron-antimeron pair spontaneously appears as the ground state of this coupled system. We also give an experimental protocol to observe these phenomena in future experiments.

DOI: 10.1103/PhysRevA.86.063628 PACS number(s): 03.75.Mn, 05.30.Jp, 67.85.Fg, 67.85.Jk

I. INTRODUCTION

One of the many interesting aspects of the field of cold atoms is that one can induce the so-called "synthetic non-Abelian gauge fields" in real experiments [1–7]. Experiments with the engineering of synthetic electromagnetism in ultracold atomic gases has recently drawn considerable theoretical attention [8–10], with a number of papers addressing schemes by which to create spin-orbit (SO) coupling in pseudo spin-$\frac{1}{2}$ and spin-1 Bose gas. Thus it opens up a new avenue to study some uncharted territory in condensed-matter physics using cold atomic gases, which are central to many exotic phenomena such as quantum Hall effect, topological insulators, and superconductivity [11–17]. In a very recent theoretical work, Wang *et al.* have shown that the condensate wave function will develop a nontrivial structure; depending on spin-dependent interaction, the ground state of a homogeneous two-component BEC with SO coupling shows a single "plane wave phase" or a "standing wave phase" (SW) [18].

In a realistic physical system, ultracold atomic gases are trapped by an external potential [19]. The spin-orbit-coupled weakly interacting BECs in harmonic traps, with or without rotation, are studied in [20–24]. For example, in Ref. [20] quantum states with Skyrmion lattice patterns emerge spontaneously and preserve either parity symmetry or combined parity-time-reversal symmetry. Furthermore, the effects of SO coupling, confinement, and interatomic interactions are studied in [21], where interesting phases are obtained for different interactions.

In the absence of SO coupling, a number of properties of the system under consideration are determined by the single-particle energy, the intracomponent interaction, and the intercomponent interaction. For example, in the strong interaction region, the actual symmetry of the ground state results from competition between the intra- and intercomponent interaction strengths. In such a system, the intracomponent interaction favors the maximum possible spread of the two gases within the system, whereas the intercomponent interaction favors the minimization of their spatial overlap. Meanwhile, designing various external potentials, such as toroidal trapping potential [25–29], vertically [30] and concentrically [31] coupled double-ring traps, single ring [32] are within current experimental capacity. When the mixtures of Bose gases are confined in a concentrically coupled annular trap, various ground phases are observed by varying the interaction strength between atoms, and the system will show a number of phase transitions [33–36].

The extra degree of freedom is introduced when the SO coupling is included. Thus, we pose the following question: What is the combined effect of the nonlinear interactions and the spin-orbit coupling on the ground state and phase transition of the spin-orbit-coupled Bose-Einstein condensates confined in concentrically coupled annular traps? In this paper, we aim to answer the above question. We demonstrate numerically that spin-orbit-coupled Bose-Einstein condensates confined in concentrically coupled annular traps support exotic ground-state configurations, and the spin-orbit coupling acts like a "switch" which can induce various phase transitions between azimuthal phase separation and phase coexistence or radial phase separation.

The paper is organized as follows. In Sec. II we formulate the theoretical model describing the spin-orbit-coupled Bose-Einstein condensates confined in concentrically coupled annular traps, and briefly introduce the numerical method. Various ground-state phases and the effect of spin-orbit coupling are discussed in Sec. III. Then the spin texture and experimental realization are presented in Sec. IV. Finally, in Sec. V, the main results of the paper are summarized.

II. MODEL AND METHOD

To begin with, we consider quasi-two-dimensional spin-orbit-coupled Bose-Einstein condensates. The model under

*szhang@ntsc.ac.cn

consideration is $\hat{H} = \hat{H}_0 + \hat{H}_{\rm int}$, where

$$\hat{H}_0 = \int d^2\mathbf{r}\,\hat{\psi}^\dagger[-\hbar^2\nabla^2/(2m) + V(\mathbf{r}) + \mathcal{V}_{\rm SO}]\hat{\psi},$$
$$\hat{H}_{\rm int} = \int d^2\mathbf{r}[g_1\hat{n}_\uparrow^2 + g_2\hat{n}_\downarrow^2 + 2g_{12}\hat{n}_\uparrow\hat{n}_\downarrow], \quad (1)$$

where m is the atom mass and assumed to be equal for the two components. $\hat{\psi} = [\hat{\psi}_\uparrow(\mathbf{r}),\hat{\psi}_\downarrow(\mathbf{r})]^T$ denotes collectively the spinor Bose field operators, and $\hat{n}_\uparrow = \hat{\psi}_\uparrow^\dagger\hat{\psi}_\uparrow, \hat{n}_\downarrow = \hat{\psi}_\downarrow^\dagger\hat{\psi}_\downarrow$. V(**r**) is the external potential and will be given explicitly below. In the present study, we consider a Rashba-type SO coupling. In this case, $\mathcal{V}_{\rm SO} = -i\lambda_R(\partial_y\hat{\sigma}_x - \partial_x\hat{\sigma}_y)$ with $\hat{\sigma}_{x,y,z}$ being the Pauli matrices and λ_R describes the SO coupling strength. For simplicity, we only focus on the special case with $g_1 = g_2 = g > 0$. Under this condition, the interaction Hamiltonian can be rewritten as $\hat{H}_{\rm int} = \int d^2\mathbf{r}(\frac{c_0}{2}\hat{n}^2 + \frac{c_2}{2}\hat{S}_z^2)$ with $\hat{n} = \hat{n}_\uparrow + \hat{n}_\downarrow$, $\hat{S}_z = \hat{n}_\uparrow - \hat{n}_\downarrow$, $c_0 = g + g_{12}$, and $c_2 = g - g_{12}$. In a recent work [10], a SO-coupled spin-$\frac{1}{2}$ ^{87}Rb BEC was realized by selecting two internal "spin" states from a spin-1 Bose gas of ^{87}Rb atoms with $F = 1$ ground electronic manifold, and the strength of SO coupling can be controlled through optical means. Furthermore, the first component is labeled with spin up in the language of pseudo spin-$\frac{1}{2}$ BECs, and spin down for the second component. We also assume $c_0 > 0$ and $\gamma = c_2/c_0$ can be either positive or negative.

In the present work we assume the spin-orbit-coupled Bose-Einstein condensate is confined by a two-dimensional concentrically coupled annular trap, which can be written as

$$V(\mathbf{r}) = \min\left\{\tfrac{1}{2}m\omega_0^2(\mathbf{r} - R_0)^2, \tfrac{1}{2}m\omega_1^2(\mathbf{r} - R_1)^2\right\}, \quad (2)$$

where **r** is the radial coordinate in cylindrical coordinates. This two-dimensional potential can be realized by adding a very tight trapping potential along the z axis, which completely freezes out the degrees of freedom of the gases along this direction. The two (overlapping) parabolas in $V(r)$ with frequencies ω_0 and ω_1 are centered at the positions with $\mathbf{r} = R_0$ and $\mathbf{r} = R_1$, hence R_0 and R_1 label the two minima of the external potential, and ω_0 and ω_1 are the harmonic trapping frequencies for the two different parabolas. Similar concentric ring geometries have also been studied in semiconductor heterostructures and the topic of electrons in quantum rings. In order to describe the system more clearly, an intuitive picture of the external potentials is presented in Fig. 1. Similar to

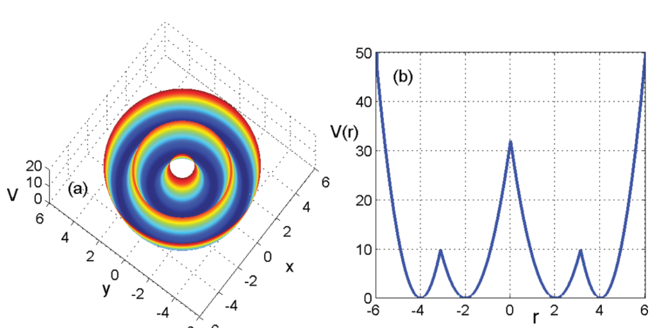

FIG. 1. (Color online) (a) Schematic of the concentrically coupled annular traps. (b) The one-dimensional plot of the external potential. **r** is in units of a_0, and V is in units of $\hbar\omega$. The other parameters are $R_0 = 2a_0$, $R_1 = 4a_0$, $\omega_0 = 4\omega$, and $\omega_1 = 5\omega$.

the work in [33], to make the product of the "width" of each annulus times the radius of each annulus comparable to each other, we must ensure that in the outer ring the potential is tighter; that is, $\omega_1 > \omega_0$. We note that our system will show the same qualitative behavior for different value choices of R_0, R_1, ω_0, and ω_1, as long as $\omega_1 > \omega_0$. Without loss of generality, the parameters in Fig. 1 are given as follows: $R_0 = 2a_0$ and $R_1 = 4a_0$ with $a_0 = [\hbar/(m\omega)]^{1/2}$ being the oscillator length, $\omega = \omega_0/4$, and $\omega_1/\omega_0 = 5/4$ (these parameters will be used throughout this paper).

III. GROUND-STATE PHASES

Let us now consider the ground-state structure of the spin-orbit-coupled Bose-Einstein condensates confined in concentrically coupled annular traps. After completion of the mean-field approximation, the Gross-Pitaevskii energy is written as

$$\xi = \int d^2r\Big\{\frac{\hbar\lambda_R}{m}[\phi_\uparrow^*(-i\partial_x - \partial_y)\phi_\downarrow + \phi_\downarrow^*(-i\partial_x + \partial_y)\phi_\uparrow] + \phi_\uparrow^*\Big(-\frac{\hbar^2}{2m}\nabla^2 + V(r)\Big)\phi_\uparrow + \phi_\downarrow^*\Big(-\frac{\hbar^2}{2m}\nabla^2 + V(r)\Big)\phi_\downarrow + \frac{c_0}{2}(|\phi_\uparrow|^2 + |\phi_\downarrow|^2)^2 + \frac{c_2}{2}(|\phi_\uparrow|^2 - |\phi_\downarrow|^2)^2\Big\}, \quad (3)$$

where the concentrically coupled annular traps $V(r)$ are given by Eq. (2). To obtain the ground state of this coupled system, the normalized gradient flow with backward Euler and second-order centered finite difference discretization within an imaginary-time propagation approach is used [37]. In our simulations, we also start with a reasonable initial state for the two components and propagate the wave functions in imaginary time to make sure that we proceed to a sufficiently large number of time steps, which guarantees that we have reached a steady state. We find that by varying the nonlinear interaction and the strength of the SO coupling, the system has various ground-state structures and shows a number of phase transitions that result from the competition between phase coexistence and radial-azimuthal phase separation, which are fundamentally different from the case with only one potential minimum, that is, a single annulus, and in a sense reminiscent of the cases in [33].

For numerical calculations, two characteristic lengths $a_0 = [\hbar/(m\omega)]^{1/2}$ and $a_\lambda = \hbar^2/(m\lambda_R)$ are introduced for the external potential and SO coupling, respectively. Hence, the unit of nonlinear interaction is $\hbar\omega a_0^2 = \hbar^2/m$, and the dimensionless SO coupling strength can be defined as $\tilde{\lambda}_{\rm SO} = a_0/a_\lambda = (m/h^3)^{1/2}\lambda_R/\omega^{1/2}$. For simplification, in this work the intercomponent interaction $g_{12} = 55$ is fixed, except that-mentioned specifically, while the intracomponent interaction can be changed using external magnetic or optical fields.

A. The effect of SO coupling on azimuthal phase separation

As in [33], by varying the interaction strength between atoms, a coupled system of two-component Bose gases that interacts with an effectively repulsive contact potential and is loaded in a concentric double annular trap reveals a series of ground-state phases in the ground state of the system. In

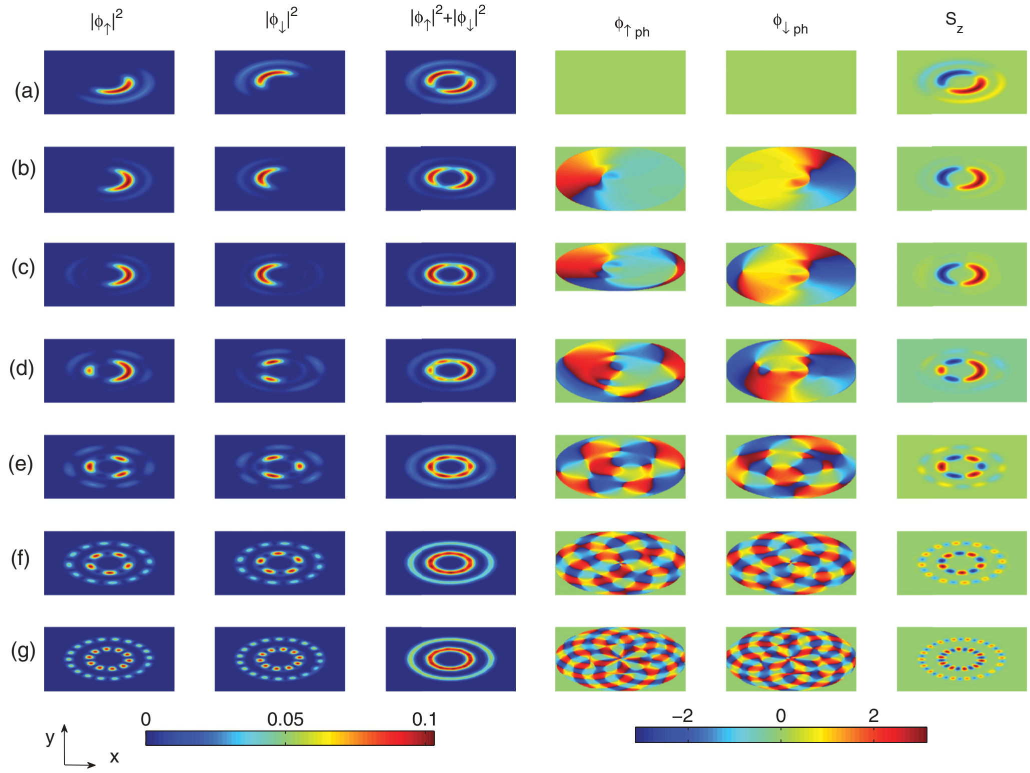

FIG. 2. (Color online) Ground-state density and phase distributions for $\phi_\uparrow(\rho,\theta)$, $\phi_\downarrow(\rho,\theta)$, and the total density (the third column) of the two components, for $g_{12} = 55$, $g = 5$, and for the spin-orbit-coupling strength $\tilde{\lambda}_{\rm SO} = 0,0.2,0.5,0.7,1,2,3$, corresponding to (a), (b), (c), (d), (e), (f), and (g), respectively. Note that the fourth and fifth columns are the phases of the spin-up and spin-down components, respectively, and the sixth column is for the pseudospin densities S_z of the total condensates. For the first row, due to the absence of spin-orbit coupling, the ground state shows azimuthal phase separation. The peaks in the densities correspond to the minima of the inner and the outer parabolas of the confining potential. The units of length and strength of SOC are $a_0 = [\hbar/(m\omega)]^{1/2}$ and $a_\lambda = \hbar^2/(m\lambda_R)$, respectively, and the scale of each figure is 6.4×6.4 in units of a_0.

the following three sections, we will start from the azimuthal phase separation regime, and perform a series of numerical experiments to study the effect of SO coupling on the ground-state density and phase distributions, and the phase transition between different phases.

Shown in the first three columns of Fig. 2 are the ground-state density distributions for $n_\uparrow(\rho,\theta) = |\phi_\uparrow(\rho,\theta)|^2$ (left), $n_\downarrow(\rho,\theta) = |\phi_\downarrow(\rho,\theta)|^2$ (middle), and the total density (right) of the two components when the system is first in the azimuthal phase separation. Figure 2(a) shows the most simple case when there is no SO coupling and the annular potential is opened. In this case, the intra- and intercomponent interactions read $g_{12} = 55$, $g = 5$, and the general phase separation condition is satisfied. Meanwhile, due to the small value of the intracomponent interaction, this repulsion interaction between the particles cannot compensate for the stronger confinement of the outer ring; hence the two components occupy mainly the inner ring and the system is close to being quasi-one-dimensional and shows azimuthal phase separation.

Figures 2(b) and 2(c) show the ground-state density distributions when the SO coupling is opened and takes a small value, such as $\tilde{\lambda}_{\rm SO} = 0.2,0.5$, for Figs. 2(b) and 2(c), respectively. From these images we observe that the inclusion of SO coupling induces the motion of the components in the inner ring with unchanged density profiles. At larger SO coupling, for example, $\tilde{\lambda}_{\rm SO} = 0.7$, the single lump for each component splits into two and a stripe develops [Fig. 2(d)].

For even larger values of SO coupling, such as $\tilde{\lambda}_{\rm SO} = 1$, 2, and 3, more lumps appear in both inner and outer rings. Examples of the ground-state density distributions in these kinds of situations are shown in Figs. 2(e)–2(g), respectively. As shown in these figures, the total density distributions of the two-component BECs to some extent spread to the outer ring. More important, the low density for one component is filled with the other component. We attribute the alternatively arranged lumps to the fact that the energy in this case is minimal, and we refer to this phase as the SW state, discovered in [18]. These phenomena can be understood by the fact that the introduction of SO coupling greatly enhances the effects of the atom-atom interactions, on one hand; and on the other hand, the inclusion of trapping potentials quantizes the radial motion for k and the azimuthal motion. More high energy atoms are repelled to the outer ring, and hence form an alternative arrangement of the two components.

More insights can be obtained if we look at the phase distributions of the two-component BECs, which are presented in the fourth and fifth columns of Fig. 2. Remarkably, the phase profile of the wave function reveals that with an increase of the strength of the SO coupling, more and more vortices appear. This behavior is in a sense reminiscent of the cases in [18],

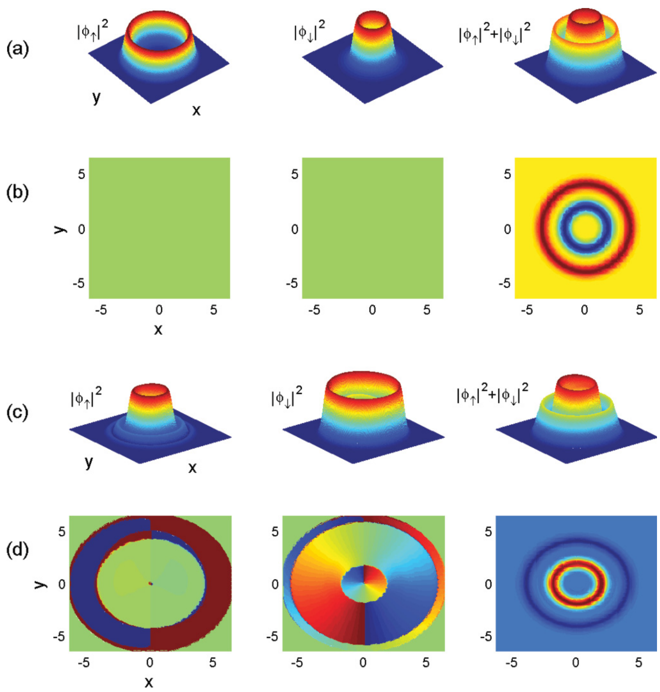

FIG. 3. (Color online) Ground-state density for $n_\uparrow(\rho,\theta) = |\phi_\uparrow(\rho,\theta)|^2$ (left), $n_\downarrow(\rho,\theta) = |\phi_\downarrow(\rho,\theta)|^2$ (middle), and the total density (right) of the two components, for $g_{12} = 55$, $g = 15$, and for the spin-orbit-coupling strength $\tilde{\lambda}_{\rm SO} = 0,1$, corresponding to (a) and (c), respectively. The corresponding phase distributions for $\phi_\uparrow$ and $\phi_\downarrow$, and the pseudospin densities S_z for the total condensates are shown in rows (b) and (d). For the first row, due to the absence of spin-orbit coupling, the ground state shows radial phase separation. The peaks in the densities correspond to the minima of the inner and the outer parabolas of the confining potential. The units of length and strength of SOC are $a_0 = [\hbar/(m\omega)]^{1/2}$ and $a_\lambda = \hbar^2/(m\lambda_R)$, respectively.

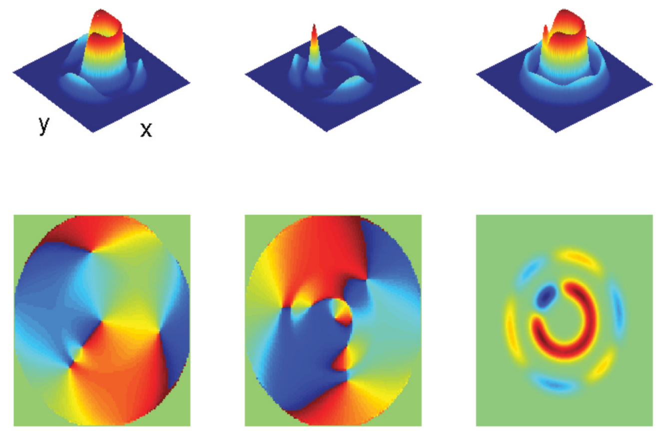

FIG. 4. (Color online) The same as in Fig. 3 but for $\tilde{\lambda}_{\rm SO} = 0.5$. In this case, a very weak SO coupling can induce a phase transition from radial phase separation to azimuthal phase separation.

where the vortex line density increases with the increase of SO coupling to minimize the single-particle energy.

B. The effect of SO coupling on radial phase separation

We now turn our attention from azimuthal phase separation to radial phase separation. When the intercomponent interaction is fixed and intracomponent is increased, a two-component Bose-Einstein condensate confined in concentrically coupled annular traps can have a phase transition, for example, from azimuthal phase separation to radial phase separation. We show in Fig. 3(a) this phase transition [as compared to Fig. 2(a) in the absence of SO coupling] for the cases $g_{12} = 55$ and $g = 15$. As shown in this figure, it is easy to see that one component occupies mainly the inner ring, while the outer ring is for the other component.

Figure 3(c) shows the ground-state density distributions when the value of SO coupling is increased to 1. It is interesting to notice that the locations of each component are exchanged with the first component occupying mainly the inner ring, while the outer ring is for the spin-down component. Since the interaction parameters $g_1 = g_2 = g$ and the particle number $N_1 = N_2$, the results will not change under the spin-component interchange, and the system shows radial phase separation in both cases. We perform a series of numerical experiments; the results show that the choice of whether the up component is in the inner ring or the outer ring is essentially random. However, if we look at the phase distributions for the two components as shown in Figs. 3(b) and 3(d), it is easy to see that the inclusion of SO effect strongly changes the phases of condensates. When the SO coupling is taken into account, not only a vortex appears but also the velocity field is fixed by the phase profile of the wave function. Very recently, the particle flow and condensate wave function for weakly trapped ultracold Bose gases with Rashba spin-orbit coupling are discussed in [38].

Figure 4 shows the density distribution when the SO coupling takes a mediate value. In this special case, a phase transition from radial phase separation to azimuthal phase separation occurs. As shown in this figure, with an increase of the value of SO coupling from zero, for example, $\tilde{\lambda}_{\rm SO} = 0.5$, most atoms of the spin-up component move to the inner ring, while the outer ring is for the spin-down component. Meanwhile, the density distribution presents azimuthal phase separation. Hence, the SO coupling has the same effect of the intracomponent interaction when the intercomponent interaction is fixed. This behavior greatly enriched the phase diagram of the two-component BECs confined in concentrically coupled annular traps, since the extra degree of freedom, SO coupling, is introduced.

Hence we conclude that when both inter- and intracomponent interactions are fixed, even a very weak SO coupling can induce a phase transition from radial phase separation to azimuthal phase separation. It reflects a well-known fact that the SO coupling can help enhance the effects of the interaction between atoms. Moreover, by further increasing the SO coupling, radial phase separation takes place again, now with the interchanged locations. Therefore, it is expected that the SO coupling, like a switch, can be used to control the phase transition between radial phase separation and azimuthal phase separation. This property may have potential applications in optical switches.

C. The effect of SO coupling on phase coexistence

With a further increase of the intracomponent interaction, the system has a phase transition from radial phase separation

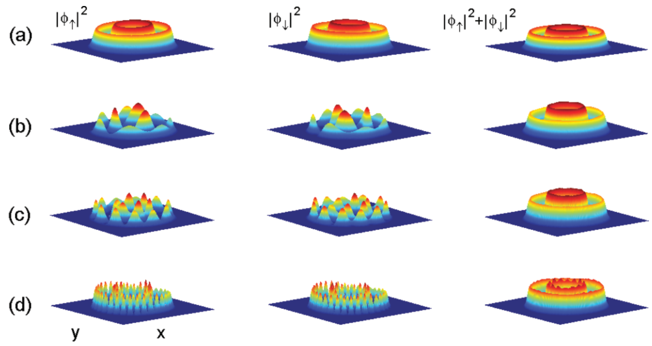

FIG. 5. (Color online) Ground-state density distributions for $n_\uparrow(\rho,\theta) = |\phi_\uparrow(\rho,\theta)|^2$ (left), $n_\downarrow(\rho,\theta) = |\phi_\downarrow(\rho,\theta)|^2$ (middle), and the total density (right) of the two components, for $g_{12} = 55$, $g = 60$, and for the spin-orbit coupling strength $\tilde{\lambda}_{\rm SO} = 0,1,2,5$, corresponding to (a), (b), (c), and (d), respectively. For the first row, due to the absence of spin-orbit coupling, the ground state shows coexistence phase. The peaks in the densities correspond to the minima of the inner and the outer parabolas of the confining potential. The units of length and strength of SOC are $a_0 = [\hbar/(m\omega)]^{1/2}$ and $a_\lambda = \hbar^2/(m\lambda_R)$, respectively, and the scale of each figure is 6.4×6.4 in units of a_0.

to phase coexistence, which is shown in Fig. 5(a). When the SO coupling is opened, this time it again changes the ground-state structure of the two components. Figures 5(b) and 6(b) show the ground-state density and phase distributions when the SO coupling takes a small value, such as $\tilde{\lambda}_{\rm SO} = 1$. Once again, we find a similar structure as compared to Fig. 2(e). However, there also exist subtle differences; for example, the total density distribution is obviously different when the SO coupling is not too large. For the azimuthal phase separation case, the total density distribution has many lumps in both inner and outer rings;, while it is uniformly distributed this time. As expected, when the SO coupling increases further, for example, from 1 to 2 or 5, more lumps appear in both rings. Examples of the ground-state density and phase distributions are shown in Figs. 5(c), 5(d) and 6(c), 6(d), respectively, with a similar argument discussed in Sec. III A.

Given the above analysis, we conclude that when both intra- and intercomponent interactions are fixed, even a very

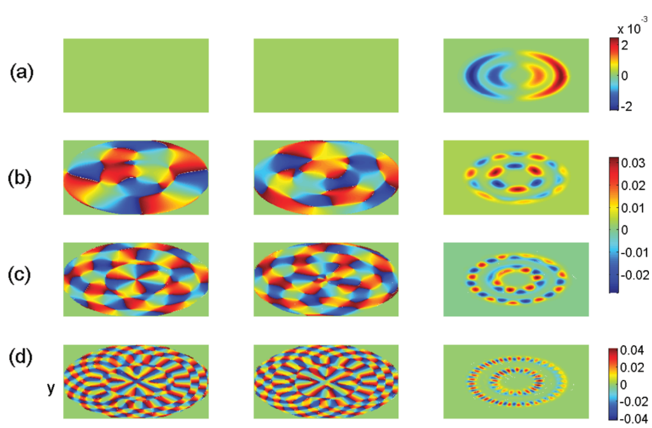

FIG. 6. (Color online) Ground-state phase distributions for $\phi_\uparrow$ (left), $\phi_\downarrow$ (middle), and the pseudospin densities S_z (right) for the total condensates, under the same conditions as those in Fig. 5.

weak SO coupling can induce a phase transition from phase coexistence or radial phase separation to azimuthal phase separation. Thus the SO coupling is likely to play a vital role in determining the ground-state phase of a spin-orbit-coupled BEC confined in concentrically coupled annular traps. It again reflects a well-known fact that the SO coupling can help enhance the effects of the interaction between atoms.

IV. SPIN TEXTURE AND EXPERIMENTAL REALIZATION

The spinor order parameter of the two-component BECs allows us to analyze this system as a pseudospin-$\frac{1}{2}$ BEC and take it as a magnetic system [39–41]. Introducing a normalized complex-valued spinor χ, we represent the two-component wave functions as $\phi_{\uparrow\downarrow} = \sqrt{\rho_T(\mathbf{r})}\chi_{\uparrow\downarrow}(\mathbf{r})$ with $\rho_T(\mathbf{r})$ the total density and the spinor satisfies $|\chi_\uparrow|^2 + |\chi_\downarrow|^2 = 1$. Hence, the pseudospin density is defined as $\mathbf{S} = \chi(\mathbf{r})^T\sigma\chi(\mathbf{r})$ with σ being the Pauli matrix. The explicit expression of $\mathbf{S} = (S_x,S_y,S_z)$ is given by

$$\begin{aligned} S_x &= (\chi_1^*\chi_2 + \chi_2^*\chi_1) = 2|\chi_1||\chi_2|\cos(\theta_1 - \theta_2),\\ S_y &= -i(\chi_1^*\chi_2 - \chi_2^*\chi_1) = -2|\chi_1||\chi_2|\sin(\theta_1 - \theta_2),\\ S_z &= |\chi_1|^2 - |\chi_2|^2, \end{aligned} \tag{4}$$

where $\theta_{1,2}$ is the phase of the wave function $\phi_{\uparrow\downarrow}$ and the modulus of the total spin is $|\mathbf{S}| = 1$. The pseudospin densities S_z are plotted in Figs. 2, 3, 4, and 6. As shown in these figures, the distributions of pseudospin S_z show similar structures with the density profiles, which can be easily seen from the last equation of Eqs. (4).

Figure 7 shows the vectorial representations of the pseudospin S projected onto the x-y plane, for $g_{12} = 55$, $g = 5$, and for the spin-orbit coupling strength $\tilde{\lambda}_{\rm SO} = 0.7,1$, corresponding to (a) and (b), respectively. Here we do not plot spin texture for the case without SO coupling, since the spin in this case always points to the z or $-z$ direction except for the interface of the two components. In the presence of SO coupling, spin texture develops after the introduction of this degree of freedom. Figure 7(a) shows the spin texture associated with the results of Fig. 2(d). We observe the emergence of a spin vortex with opposite vorticity (the in-plane magnetization has a "vortex-antivortex" structure [42]), which can de denoted as the spin vortex lattice state studied in [43]. A similar structure also appears in the strong SO coupling case, and we show in Fig. 7(b), associated with the result of Fig. 2(e), this similar spin vortex structure. Moreover, in these two cases all spin vortices exhibit a similar structure: the central spin always points to the $\pm z$ axis, while the others increasingly tilt and finally lie on the xy plane, forming a circulation pattern away from the center. We thus term this structure, shown in Fig. 7, the meron-antimeron pair, which are intrinsical excitations to the two-dimensional system. Here we want to point out that the spin texture associated with the results of Fig. 5 (not shown here for the sake of brevity) resemble those shown in Fig. 7 for the azimuthal phase separation case.

Next we turn to the radial phase separation case. Shown in Fig. 8 are the vectorial representations of the pseudospin S projected onto the x-y plane, associated with the results of Figs. 3(c) and 4. It is easy to see that even when a

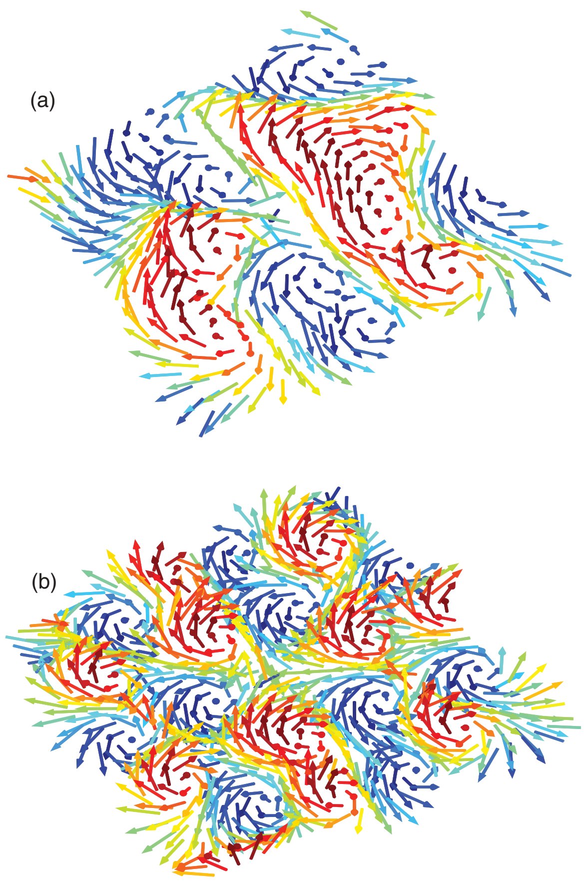

FIG. 7. (Color online) The vectorial representations of the pseudospin $\mathbf{S}$ projected onto the x-y plane, for $g_{12} = 55$, $g = 5$, and for the spin-orbit coupling strength $\tilde{\lambda}_{\text{so}} = 0.7, 1$, corresponding to (a) and (b), respectively. The colors ranging from blue to red describe the values of S_z from -1 to 1, and the scale of each figure is 6.4×6.4 in units of a_0.

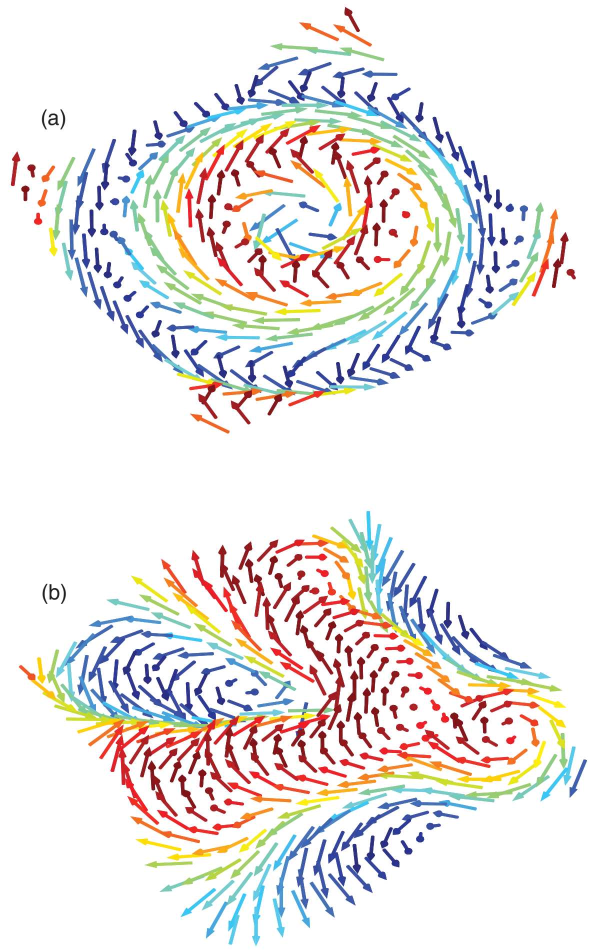

FIG. 8. (Color online) The vectorial representations of the pseudospin $\mathbf{S}$ projected onto the x-y plane, for $g_{12} = 55$, $g = 15$, and for the spin-orbit coupling strength $\tilde{\lambda}_{\text{so}} = 1, 0.5$, corresponding to (a) and (b), respectively. The colors ranging from blue to red describe the values of S_z from -1 to 1, and the scale of each figure is 6.4×6.4 in units of a_0.

small SO coupling is introduced, spin texture develops and spin vortex lattice forms. Remarkably, a giant spin vortex appears in Fig. 8(a) associated with the results of Fig. 3(c). As we mentioned in Sec. III B, although the coupled system shows radial phase separation in both Figs. 3(a) and 3(c), the phase distributions are different and thus spin texture develops. We conclude that the spin texture and spin vortex-antivortex pair are intrinsic to the spin-orbit-coupled Bose-Einstein condensates confined in concentrically coupled annular traps.

Finally, we give an experimental protocol to observe the various ground-state structures and phase transitions in possible future experiments. First, the SO-coupled spin-$\frac{1}{2}$ ^{87}Rb BECs can be realized by selecting two internal "spin" states from a spin-1 Bose gas of ^{87}Rb atoms with $F = 1$ ground electronic manifold; then the condensates can be loaded in a concentrically coupled annular trap. With regard to the parameters used in the present paper, as discussed in the typical experiment for two-dimensional spin-$\frac{1}{2}$ ^{87}Rb atoms [10], the strength of SO coupling is about 10 in our dimensionless units, and the intra- and intercomponent interaction strengths are about $10^2 \sim 10^3(\hbar\omega_\perp a_\perp^2)$ [22,44]. However, in realistic physical systems, the interactions between atoms can be controlled by modifying atomic collisions, which are experimentally feasible due to the flexible and precise control of the scattering lengths achievable by magnetically tuning the Feshbach resonances. Meanwhile, the strength of the SO coupling can be precisely controlled by optics means—from no coupling at all to strong coupling, which scales with the laser's intensity [10,45]. Hence, the parameters used in this study are within current experimental capacity. To probe the different components, we can switch off the traps and the Raman beams, and absorption image the two different components after a time of flight. Moreover, we also have examined the ground-state structures in the limiting cases with intra- or intercomponent interaction equal to zero, and for other parameters. In the two limiting cases, we find that the two components always form an alternative density arrangement, and more lumps appear with increasing the SO coupling strength. Further work can be extended to the spin-1 BECs with (or without) rotating, where more degrees of freedom are introduced and more interesting phenomena, such as meron, fractionalized skyrmion, giant vortex, and topological spin texture, can occur [46].

V. CONCLUSIONS

In summary, we have investigated a spin-orbit-coupled Bose-Einstein condensate confined in concentrically coupled annular traps. This system is investigated within the full parameter space accounts for all the nonlinear two-body collisions, together with the spin-orbit coupling. Our results show that when the SO coupling is introduced, the system presents a rich ground state structure. Moreover, we have studied the effect of interplay of nonlinear interaction and spin-orbit coupling, and found that SO coupling can enhance the interaction effects; even a small value of SO coupling can induce phase transition between different ground-state phases. With regard to the emergence of spin texture in the presence of SO coupling, our results show that a meron-antimeron pair spontaneously appears as the ground state of this coupled system, and more and more meron-antimeron pairs appear with an increase of SO coupling. These phenomena open possibilities for future applications in optical switches, and maybe arouse interest in the study of SO-coupled BECs in various external potentials.

ACKNOWLEDGMENTS

We would like to express our sincere thanks to L. Wen, S.-W. Song, and W. Han for helpful discussions. This work was supported by NSFC under Grants No. 11104064, No. 10934010, and No. 11174282; the KPNSF of China under Grant No. 10834007; the NSFDYS of China under Grant No. 61025023; the NMFSEID under Grant No. 61127901; the NKBRSF of China under Grants No. 2011CB921502 and No. 2012CB821300; and NSFC-RGC under Grants No. 11061160490 and No. 1386-N-HKU748/10.

[1] K. Osterloh, M. Baig, L. Santos, P. Zoller, and M. Lewenstein, Phys. Rev. Lett. **95**, 010403 (2005).
[2] J. Ruseckas, G. Juzeliūnas, P. Öhberg, and M. Fleischhauer, Phys. Rev. Lett. **95**, 010404 (2005).
[3] I. I. Satija, D. C. Dakin, and C. W. Clark, Phys. Rev. Lett. **97**, 216401 (2006).
[4] S. L. Zhu, H. Fu, C. J. Wu, S. C. Zhang, and L. M. Duan, Phys. Rev. Lett. **97**, 240401 (2006).
[5] X. J. Liu, X. Liu, L. C. Kwek, and C. H. Oh, Phys. Rev. Lett. **98**, 026602 (2007).
[6] T. D. Stanescu, C. Zhang, and V. Galitski, Phys. Rev. Lett. **99**, 110403 (2007).
[7] G. Juzeliūnas, J. Ruseckas, and J. Dalibard, Phys. Rev. A **81**, 053403 (2010).
[8] Y.-J. Lin, R. L. Compton, K. Jimnez-Garca, J. V. Porto, and I. B. Spielman, Nature (London) **462**, 628 (2009).
[9] Y.-J. Lin, R. L. Compton, A. R. Perry, W. D. Phillips, J. V. Porto, and I. B. Spielman, Phys. Rev. Lett. **102**, 130401 (2009).
[10] Y.-J. Lin, K. Jiménez-García, and I. B. Spielman, Nature (London) **471**, 83 (2011).
[11] T. D. Stanescu, B. Anderson, and V. Galitski, Phys. Rev. A **78**, 023616 (2008).
[12] M. Merkl, A. Jacob, F. E. Zimmer, P. Öhberg, and L. Santos, Phys. Rev. Lett. **104**, 073603 (2010).
[13] J. Larson, J. P. Martikainen, A. Collin, and E. Sjoqvist, Phys. Rev. A **82**, 043620 (2010).
[14] C. Wu and I. Mondragon-Shem, Chin. Phys. Lett. **28**, 097102 (2011).
[15] T.-L. Ho and S. Zhang, Phys. Rev. Lett. **107**, 150403 (2011).
[16] X.-Q. Xu and J. H. Han, Phys. Rev. Lett. **108**, 185301 (2012).
[17] R. Liao, Y. Yi-Xiang, and W. M. Liu, Phys. Rev. Lett. **108**, 080406 (2012).
[18] C. Wang, C. Gao, C.-M. Jian, and H. Zhai, Phys. Rev. Lett. **105**, 160403 (2010); H. Zhai, Int. J. Mod. Phys. B **26**, 1230001 (2012).
[19] X. F. Zhang, Q. Yang, J. F. Zhang, X. Z. Chen, and W. M. Liu, Phys. Rev. A **77**, 023613 (2008); X. F. Zhang, X. H. Hu, X. X. Liu, and W. M. Liu, *ibid.* **79**, 033630 (2009).
[20] H. Hu, B. Ramachandhran, H. Pu, and X.-J. Liu, Phys. Rev. Lett. **108**, 010402 (2012).
[21] S. Sinha, R. Nath, and L. Santos, Phys. Rev. Lett. **107**, 270401 (2011).
[22] B. Ramachandhran, B. Opanchuk, X.-J. Liu, H. Pu, P. D. Drummond, and H. Hu, Phys. Rev. A **85**, 023606 (2012).
[23] H. Hu and X.-J. Liu, Phys. Rev. A **85**, 013619 (2012).
[24] X.-Q. Xu and J. H. Han, Phys. Rev. Lett. **107**, 200401 (2011).
[25] S. Gupta, K. W. Murch, K. L. Moore, T. P. Purdy, and D. M. Stamper-Kurn, Phys. Rev. Lett. **95**, 143201 (2005).
[26] S. E. Olson, M. L. Terraciano, M. Bashkansky, and F. K. Fatemi, Phys. Rev. A **76**, 061404(R) (2007).
[27] I. Lesanovsky and W. von Klitzing, Phys. Rev. Lett. **99**, 083001 (2007).
[28] C. Ryu, M. F. Andersen, P. Cladé, V. Natarajan, K. Helmerson, and W. D. Phillips, Phys. Rev. Lett. **99**, 260401 (2007).
[29] K. Henderson, C. Ryu, C. MacCormick, and M. G. Boshier, New J. Phys. **11**, 043030 (2009).
[30] I. Lesanovsky and W. von Klitzing, Phys. Rev. Lett. **98**, 050401 (2007).
[31] J. Brand, T. J. Haigh, and U. Zülicke, Phys. Rev. A **80**, 011602(R) (2009).
[32] J. Smyrnakis, S. Bargi, G. M. Kavoulakis, M. Magiropoulos, K. Kärkkäinen, and S. M. Reimann, Phys. Rev. Lett. **103**, 100404 (2009).
[33] F. Malet, G. M. Kavoulakis, and S. M. Reimann, Phys. Rev. A **81**, 013630 (2010).
[34] P. Ao and S. T. Chui, Phys. Rev. A **58**, 4836 (1998).
[35] E. Timmermans, Phys. Rev. Lett. **81**, 5718 (1998).
[36] C. J. Pethick and H. Smith, *Bose-Einstein Condensation in Dilute Gases* (Cambridge University Press, Cambridge, UK, 2002).
[37] W. Z. Bao and W. J. Tang, J. Comput. Phys. **187**, 230 (2003); W. Z. Bao and J. Shen, SIAM J. Sci. Comput. **25**, 1674 (2004); W. Z. Bao, Multiscale Model. Simul. **2**, 210 (2004); W. Bao, H. Wang, P. A. Markowich, Comm. Math. Sci. **3**, 57 (2005).
[38] T. Ozawa and G. Baym, Phys. Rev. A **85**, 063623 (2012).
[39] K. Kasamatsu, M. Tsubota, and M. Ueda, Phys. Rev. A **71**, 043611 (2005).

[40] M. Ueda, *Fundamentals and New Frontiers of Bose-Einstein Condensation* (World Scientific, Singapore, 2010).
[41] W. Han, S. Y. Zhang, J. J. Jin, and W. M. Liu, Phys. Rev. A **85**, 043626 (2012).
[42] D. Solenov, D. Mozyrsky, and I. Martin, Phys. Rev. Lett. **108**, 096403 (2012).
[43] S.-W. Su, I.-K. Liu, Y.-C. Tsai, W. M. Liu, and S.-C. Gou, Phys. Rev. A **86**, 023601 (2012).
[44] T. Yefsah, R. Desbuquois, L. Chomaz, K. J. Gunter, and J. Dalibard, Phys. Rev. Lett. **107**, 130401 (2011).
[45] M. Chapman and C. Sá de Melo, Nature (London) **471**, 41 (2011).
[46] T. Kawakami, T. Mizushima, M. Nitta, and K. Machida, Phys. Rev. Lett. **109**, 015301 (2012); M. Nitta, K. Kasamatsu, M. Tsubota, and H. Takeuchi, Phys. Rev. A **85**, 053639 (2012).